LAWRENCE
LIVERMORE
NATIONAL
LABORATORY

LLNL-JRNL-407023

High Energy, Short Pulse Fiber Injection Lasers at Lawrence Livermore National Laboratory

J. W. Dawson, M. J. Messerly, H. H. Phan, J. K. Crane, R. J. Beach, C. W. Siders, C. P. J. Barty

September 16, 2008

IEEE Journal of Selected Topics in Quantum Electronics

Disclaimer

High Energy, Short Pulse Fiber Injection Lasers at Lawrence Livermore National Laboratory

Jay W. Dawson, *Member, IEEE*, Michael J. Messerly, Henry H. Phan, John K. Crane, Raymond J. Beach, Craig W. Siders and C. P. J. Barty

***Abstract*—A short pulse fiber injection laser for the Advanced Radiographic Capability (ARC) on the National Ignition Facility (NIF) has been developed at Lawrence Livermore National Laboratory (LLNL). This system produces 100 μJ pulses with 5 nm of bandwidth centered at 1053 nm. The pulses are stretched to 2.5 ns and have been recompressed to sub-ps pulse widths. A key feature of the system is that the pre-pulse power contrast ratio exceeds 80 dB. The system can also precisely adjust the final recompressed pulse width and timing and has been designed for reliable, hands free operation. The key challenges in constructing this system were control of the signal to noise ratio, dispersion management and managing the impact of self phase modulation on the chirped pulse.**

***Index Terms*—Laser fusion, Optical fiber lasers, Ultrafast optics**

I. Introduction

Fiber lasers have been shown to be an extremely promising technology for scaling to very high average powers (kWs) with excellent beam quality [1]-[4]. This property of fiber lasers is predominantly attributable to the low loss single mode or near single mode waveguide that acts as a continuous spatial filter, naturally incorporating a high surface area to volume ratio for thermal management. Sadly, the very features that enable straightforward scaling of average power preclude scaling to very high pulse energies. Though up to 4 mJ/ns pulses have been achieved [5], this is small compared to the output of the NIF bulk laser system, which can produce up to 20kJ/pulse in a few ns in a single beam line [6]. In order to achieve desired pulse energies, post fiber amplification in a bulk laser system must generally be employed.

Bulk, fiber-based and hybrid systems designed to produce high-energy short pulses typically employ chirped pulse amplification (CPA) [7] to minimize system non-linearities. The great advantage of hybrid systems is that the fiber system replaces what is typically the most problematic portion of a high-energy system, the injection laser, and provides stable pointing, excellent beam quality and robust, reliable operation with minimal user maintenance.

The National Ignition Facility (NIF) at Lawrence Livermore National Laboratory (LLNL) already employs a fiber laser system to generate its nanosecond length pulses with precise spectral control, temporal pulse shaping and timing for all 192-beam lines. The NIF facility will produce 1.8MJ of total energy at 351 nm. This 1.8 MJ of energy will be focused onto a deuterium-tritium target in order to produce an inertial fusion reaction that releases more energy than it consumes.

Recently the need has arisen to convert one or more beam lines of the NIF laser to generate high-energy short pulses. These short pulse beam lines will serve a variety of missions including providing an X-ray backlight for directly observing the hydrogen pellet implosions via a system known as the Advanced Radiographic Capability (ARC) [8] and providing short, high-energy pulses for "fast ignition" experiments [9].

In order to convert a NIF beamline to short pulse operation three modifications are required. First, a grating based pulse compressor must be added to the end of the beamline. Due the difficulty and expense of producing the large gratings required for the pulse compressor, each NIF beam line configured for short pulse operation will be split into two sub-apertures, a solution referred to hereafter as "split beam" operation [8]. While this has the disadvantage of reducing the total energy in each aperture by slightly more than two, it has the advantage of providing twice as many short pulses with which to perform radiography. In order to seed split beam injection properly, it is necessary to alter the injection system via modification of the pre-amplifier module (PAM) by the addition of a split beam injection system (SBI). These modifications have been discussed in detail elsewhere [8]. This paper will focus on the third modification, the construction of a fiber injection laser system to generate the short pulses, stretch them for CPA, provide independent timing and pulse width control for each sub-aperture, transmit the seed pulses from the master oscillator room (MOR) to the main laser bay and amplify the pulses to 100 μJ for injection into the main NIF laser via the SBI system. NIF will then amplify the pulse in each sub-aperture up to 1kJ (limited by damage on the final optics). The recompressed pulses will be independently focused to backlighter targets near the main target for the radiography mission.

There has been significant interest in short pulse fiber laser systems for machining and other applications [10], [11]. Mode-locked fiber lasers at 1μm and 1.5μm capable of

Manuscript received September 1, 2008. This work performed under the auspices of the U.S. Department of Energy by Lawrence Livermore National Laboratory under Contract DE-AC52-07NA27344.

J. W. Dawson, M. J. Messerly, H. H. Phan, J. K. Crane, R. J. Beach, C. W. Siders and C. P. J. Barty are with the Lawrence Livermore National Laboratory, Livermore, CA 94550 USA (phone: 925-422-1617; fax: 925-423-6195; e-mail: dawson17@llnl.gov).

generating pulses widths as short as 33 fs and pulse energies as large as 265 nJs have been demonstrated [12]-[14]. CPA systems have been demonstrated with mJ pulse energies and average powers of greater than 100W [15], [16]. Systems employing chirped fiber Bragg gratings (CFBGs) as the CPA stretcher with the CFBG dispersion designed to be matched to that of a Traecy compressor [17], [18] have also been demonstrated. However, few references have discussed hybrid bulk/fiber CPA systems or presented specific requirements of a fiber injection laser for very high energy, petawatt class laser systems [19].

This paper reviews the development of a short pulse fiber injection laser for NIF, including issues that may be encountered in constructing a hybrid fiber/bulk CPA system. The paper is organized as follows: section II discusses the injection laser requirements for the ARC system on NIF, section III provides an overview of the system including a discussion of the impact of the requirements on the system design, section IV reviews data from key sub-systems, section V shows recompressed pulse results obtained by compressing the output of the fiber system in a table-top compressor, section VI reviews the design of the pulse tweaker based upon the results of section V and section VII provides a brief conclusion.

II. Key System Requirements

The primary rationale in constructing a fiber injection laser system is that by basing the system on optical fiber technology it will be more robust, reliable and stable than other alternatives. Not all components of a fiber laser system are easily constructed from optical fibers. For example, even telecom optical isolators remain hybrid fiber/micro-optic devices; thus it is expected that in a CPA system some components may also need to be hybrids. One requirement of the system is to minimize the number of hybrid components and make remaining hybrids as compact and robust as possible.

The NIF amplifier chain is comprised of Nd-doped phosphate glass that has a 1053.0 nm center wavelength (as measured in air) and a bandwidth of 2.2nm at the full width half maximum (FWHM). The requirement for the ARC injection laser system is to have a center wavelength of 1053.0 nm in air with a bandwidth of 5nm. This ensures the full bandwidth of NIF will be seeded without throwing away too much excess energy.

Timing control in a large laser system is very important. The goal of the ARC diagnostic is to take a radiographic picture at one or more specific times during the implosion of the principal target. In order to achieve this, the system must be synchronized to an external master clock. It is also desired to be able to time the sub-apertures of the split beam independently. Requirements for the ARC system are absolute pulse timing control of 12ps RMS relative to the NIF master clock and control of the split beam sub-apertures to 0-20 ns relative to each other with 1 ps resolution. The former requirement implies that the injection laser system mode-locked oscillator must be phase locked to a multiple or sub-multiple of the NIF master clock. The sub-apertures require a means for providing an independent delay relative to each other.

In any CPA system, control of the overall system dispersion is critical. The fiber injection laser system will generate the initial pulse and provide the bulk of the positive dispersion via both its pulse stretcher and the large amount of glass encompassed in the fiber transport and amplification components. In order to provide transform-limited pulses at the output of the system it is necessary that the pulse stretcher compensate for the overall system dispersion including the final compressor and the dispersion of all of the material between the oscillator and the grating pulse compressor. The ARC system has two additional requirements. First it must be able to adjust the final output pulse width from its transform limit up to 60ps. This is because the system output is damage limited by the final optic in the compressor, whose damage threshold increases with increasing pulse width. Not all missions require picosecond pulses; thus being able to adjust the pulse width means more energy can be extracted from the system for those missions that employ longer pulses. In smaller systems pulse width is generally controlled by tuning the compressor; in ARC, the compressor consists of meter scale optics in a vacuum vessel. Thus it is easier to control the overall system dispersion in the injection laser than by adjusting the compressor. Further, the two split beam compressors will not be guaranteed to be identical. In fact, in order to maximize the amount of the total NIF aperture that can be accessed they were deliberately designed to be slightly different. Thus it is desired to have independent control of the dispersion of the two split beams.

At 1kJ per sub-aperture pulse energy, even pre-pulses that contain a small fraction of the main pulse's energy can prematurely damage a target. Thus pre-pulse power contrast is a critical requirement. For the ARC system, a pre-pulse power contrast ratio of 80 dB has been set as a requirement. This only applies to energy that precedes the main pulse (prepulses and amplified spontaneous emission (ASE)) by a few hundred ps out to 5-10 ns. Power closer to the main pulse is less important since the target will not have enough time to respond before the arrival of the main pulse. For any high-energy laser system, pre-pulse contrast will be a requirement. Some applications, such as fast ignition may have even more stringent requirements.

The final injection laser requirement is pulse energy. The pulses out of the injection laser need to have sufficient energy to seed the main laser and extract the required energy. For the ARC system, 100 μJ per sub-aperture was determined to be a minimum requirement.

III. Overview of System Design

Figure 1 is a block diagram of the system. The starting point is a fiber-based mode locked oscillator that is phase locked to an external clock. The system is constructed completely from polarization maintaining (PM) optical fiber with the single exception of the chirped fiber Bragg grating (CFBG). To meet the pre-pulse contrast requirements discussed in section II, a

clean stretched pulse with a minimum energy of 1 nJ must be injected into the amplifier chain (See section III-B below).

Achieving a pulse with 5 nm of bandwidth and 1 nJ of pulse energy with 80dB of pre-pulse contrast after the pulse stretcher (and its losses) while maintaining the design goal of a compact fiber system adds significant complexity to the system. The 40 m of PM fiber, compressed pulse amplifier, pulse compressor, amplified spontaneous emission (ASE) pulse cleaner and pre-stretcher were added to the system design for this purpose. These components control the pulse bandwidth, boost the pulse to a high energy in a mini-CPA system, remove the resulting ASE from that CPA system and pre-stretch the pulse to minimize non-linear effects in the fiber pulse stretcher.

The fiber pulse stretcher is a CFBG custom produced for this system by the University of Southampton. It stretches the pulse to 2.5 ns, corrects the chromatic dispersion of the glass in the system-wide optical path, and corrects the residual third order dispersion of the pulse compressor.

The pulse is amplified and split into independent beam lines for the two sub-apertures. Pulse tweakers then adjust the precise timing and dispersion of the pulses for each split beam sub-aperture. Patch cords of varying length can be inserted to provide gross timing adjustment, and the tweaker itself provides fine timing adjustment in the 1ps-3ns range.

To this point the system will be contained in the NIF master oscillator room (MOR), an easily accessible location. The pulses are then transported through a 120 m PM fiber, to carry them near the bulk amplifier chain. Before injection into bulk amplifiers, their energy is boosted to the required 100 μJ level by a pair of concatenated fiber amplifiers. Amplification after transport minimizes potential nonlinear artifacts.

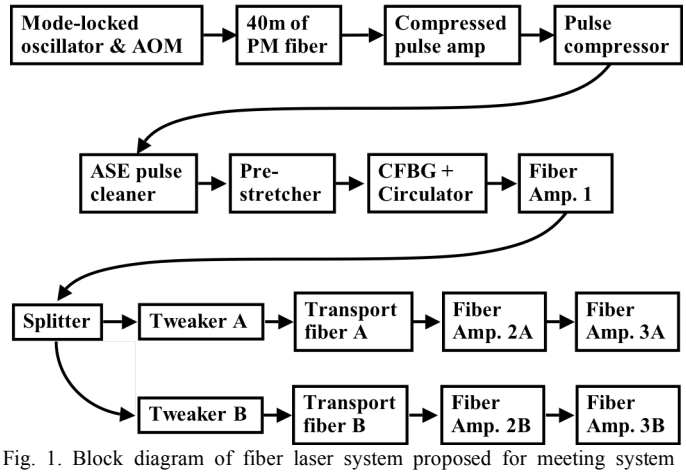

Fig. 1. Block diagram of fiber laser system proposed for meeting system requirements detailed in section II.

The fiber system faces several potential challenges, particularly, dispersion, pre-pulse contrast, possible group delay ripple in the CFBG, self-phase modulation (SPM) non-linearity in the transport fibers and the final amplifiers, and the interaction of CFBG imperfections with SPM. The dispersion, pre-pulse contrast and SPM theoretical estimates made prior to the system construction discussed this section and experimental results are reviewed in the following two sections.

A. System Dispersion Roll-up

Dispersion control in the system essentially reduces to good bookkeeping. Unfortunately, the dispersive characteristics of fiber components are rarely known to the level required for ultra-fast laser systems. Thus, the initial system layout was based upon estimates, which were refined as it was built.

The pulse is compressed to its transform limit at the output of the ASE pulse cleaner shown in Fig. 1; thus the dispersion calculation begins here. The pre-stretcher is a grating pulse compressor constructed from two 1780 g/mm gratings with an angle of incidence of 85 degrees and a slant distance between the gratings of 6.12 cm as measured parallel to the diffracted center wavelength beam. The estimated group delay dispersion (GDD) of the pre-stretcher is -3.5 ps^2/rad and the third order dispersion (TOD) is 0.0481 ps^3/rad^2. The goal of this component is to reduce the pulse intensity prior the CFBG in order to avoid strong SPM effects inside the CFBG. While the CFBG provides GDD of the opposite sign as that of the pre-stretcher, the pulse never recompresses inside the CFBG. One way to think of this is to consider that at the output of the pre-stretcher, the blue wavelength components of the pulse lead the red wavelength components. In the CFBG the red wavelength components are reflected at the near end of the CFBG and the blue wavelength components are reflected from the far end of the CFBG, which is longer than the length of the pre-stretched pulse. Therefore red wavelength components are systematically stripped away from the trailing edge of the pulse so that pulse never returns to its transform limit while traversing the CFBG.

Though the path length of the fiber-based components is tens of meters, the material dispersion is relatively small compared to the amount applied to stretch the pulse. Including the amplifiers and transport fiber, as well as the glass in the NIF amplifier chain, the GDD of the material was estimated to be 2.1 ps^2/rad and the TOD to be 0.0049 ps^3/rad^2. The ARC compressor was originally planned to have a GDD of -279.4 ps^2/rad and a TOD of 4.17 ps^3/rad^2. Based upon this estimate, the CFBG was specified to have a GDD of 313.0 ps^2/rad and a TOD of -4.849 ps^3/rad^2.

The tweaker was designed to provide a tunable GDD up to -32.2 ps^2/rad and TOD of 0.627 ps^3/rad^2. The groove density of the tweaker gratings is 1780g/mm leading to an angle of incidence of 73.5 degrees and a slant distance between gratings of 79.6 cm. The tweaker dispersion range was designed to be large enough to accommodate anticipated future needs. Moreover, it was designed so that the shortest pulses occurred at the maximum dispersion. A problem for a system such as ARC is how to create a diagnostic suite that can accurately measure all of the properties of the output pulse on each shot when the pulse width and peak intensity may change by up to 100X. This issue was resolved by choosing to set the pulse tweaker to its maximum value for transform limited pulses and then reduce the grating separation to create longer pulses. A second tweaker in the diagnostic suite can then add in the missing dispersion to bring the pulse back to its transform limit at the diagnostics for each shot.

B. Pre-Pulse Contrast

As defined here, pre-pulse contrast is essentially signal-to-noise ratio where the signal is the peak compressed pulse power and the noise is the ASE. At the output of the ARC system there will be a 1 kJ pulse compressed to 1 ps FWHM, implying a peak power of 1 PW (10^{15} W). Given a desired signal to noise ratio of 80 dB or 10^8, this implies the ASE preceding the pulse needs to be less than 10 MW peak power over 0.1-5ns just prior to the arrival of the pulse. (In terms of power this would not appear to be aggressive, but recall this power over several ns is only 10-50 mJ compared to an amplified pulse energy of 1kJ.) From Giles and Desurvire [25] the ASE in a fiber amplifier is equal to

$$P_{ASE} = 2 \cdot n_{sp} \cdot (G-1) \cdot h\nu \cdot \Delta\nu \qquad (1)$$

where P_{ASE} is the amplified spontaneous emission power, n_{sp} is the spontaneous photon number (n_{sp} = 1.2 for Yb^{3+} fiber amplifiers, but is amplifier dependent), G is the system gain, h is Plank's constant, ν is the signal center frequency and $\Delta\nu$ is the system's spectral bandwidth. For P_{ASE} = 10 MW at 1053nm with 5 nm bandwidth, Eq. 1 requires G=125 dB. If the output energy is 1 kJ, then the minimum input pulse energy must be 0.3nJ to achieve the desired 80dB pre-pulse contrast ratio. This was rounded up to 1nJ in the final requirements to provide some margin for errors.

C. Self Phase Modulation

SPM of chirped pulses in CPA systems is known to degrade system pulse quality [20], [21]. It can be quantified with the equation [20],

$$B = \frac{2\pi}{\lambda} \int n_2 \cdot I \cdot dz \qquad (2)$$

where B represents the "B-integral" parameter, λ is the center wavelength of the signal, n_2 is the non-linear index of the material (3 X 10^{-20} m^2/W in silica), I is the signal intensity and the integration is over the full signal path. In optical fiber amplifiers the mode field diameter is essentially constant with distance and the signal tends to grow exponentially with distance, so Eq. 2 can be integrated directly to obtain,

$$B = \frac{2\pi}{\lambda} n_2 \cdot \left(\frac{P}{\pi a^2} \right) \cdot L_{eff} \qquad (3)$$

where P is the input power at the peak of the pulse, a is the mode field radius of the fiber mode and L_{eff} is the effective length of the optical fiber given by,

$$L_{eff} = \frac{G-1}{\ln(G)} L \qquad (4)$$

where L is the fiber length and G is the linear gain of the full length of fiber.

Using Eqs. 3 and 4, the B-integral parameter for all of the components in the system in figure 1 were calculated. Only three components in the system contribute significantly to the net B-integral; the transport fiber and fiber amplifiers 2 and 3. The dominant source of B-integral is amplifier 3.

The transport fibers are 120 m long, PM fibers with a 6.6 μm mode field diameter carrying 1nJ pulses stretched to 2.5ns, making the B-integral for the transport fiber 0.25 radians.

Fiber amplifier 2 has a input pulse energy of 1nJ and a gain of 30dB. It is constructed from 2.74 m of gain fiber with 0.3m of passive fiber for the output connector both fibers have a mode field diameter of 11 μm. Thus the accumulated B-integral for amplifier 2 is 0.53 radians.

Nufern supplied amplifier 3, and due to the high pulse energy it generates it was designed to minimize the B-integral, even at the expense of efficiency. The amplifier provides 20dB of gain and is constructed from 1.5m of passive fiber followed by 1.25 m of gain fiber both having a mode field diameter of 22μm. At 1μJ input, this yields a B-integral of 5.3 radians.

Including the relatively small B-integral contributions of other components, it is estimated that the total accumulated B-integral in the system is 6.1 radians. This is a relatively large value for a CPA system for pulses that are Gaussian in the time domain. Here though the pulses are not Gaussian; the oscillator has a spectral bandwidth of 30nm that is clipped to 5nm by the CFBG. Thus the temporal shape of the pulse propagating through the fiber is nearly square, and ideally the B-integral consequently only changes (accumulates) near its leading and trailing edges, not through its center. However, since the pulse's spectrum is much wider than NIF's bulk amplifiers spectra (5 nm vs. 2.2 nm), any distortions to the leading and trailing edges have little effect on the shape of the amplified pulse. Simulations imply the edge distortions generate an inconsequential pedestal in the range of 50-100ps.

In addition to the classical concerns about B-integral, the system also encountered issues of the SPM non-linearity interacting with the CFBG group delay ripple, an issue that was not anticipated when the system was designed, but was observed in testing. A theoretical explanation of this effect has recently been presented [21].

IV. Experimental Data From Critical Components

This section reviews relevant data of the as built system with emphasis on the mode-locked fiber oscillator, the ASE pulse cleaner, the CFBG and the amplifier chain.

A. Mode-locked fiber laser

The fiber mode-locked oscillator is based upon the self-similar oscillator design developed at Cornell [12]; a schematic of the oscillator is shown in figure 2a. The pump diode was a fiber coupled 500mW 976nm diode made by JDS Uniphase. The wavelength division multiplexer (WDM) was a 3m fused fiber coupler made by SIFAM (L2SWM980/1053X-SFO103) to combine 976nm light with 1053nm light. The Yb^{3+} fiber was made by INO (part number Yb 198); it is 2m long with a mode field diameter of 2.8 μm. The fiber ports, isolator, waveplates and polarization beam splitter were all made by OFR (part numbers PAF-X-7, IOB-2D-1053-VLP, RZB-1/2-1053, PSCL-B-VR-1053). The gold gratings for the dispersion compensation delay line were made by Newport Corporation and were 600g/mm optimized at 1μm wavelength (part number 53004BK02-520R). The angle of incidence into the dispersion compensating delay line was 30 degrees and the approximate slant distance between the gratings was 6.8cm. A

roof mirror permits double passing the gratings and conveniently changes the beam height so that the beam only encounters the polarization beam splitter once. The roof mirror stage contains a long travel motorized actuator (Newport part number AD-100). The grating stage (ThorLabs part number NF5DP20) contains a PZT actuator. When phase locking, the slower actuator compensates for environmental changes such as long term temperature drift and the PZT compensates for faster fluctuations inside the cavity. The combination of Yb^{3+} fiber length and the waveplate settings were adjusted in order to maximize the oscillator spectrum at 1053nm.

The operating oscillator center wavelength is 1052 nm, it has 35.5 nm bandwidth (FWHM) see Fig. 3. The oscillator repetition rate is 38.88 MHz. The pulses emitted by the oscillator are positively chirped to a pulse width of 4-5 ps, but may be recompressed to less than 100 fs with a standard grating compressor (this was verified with a Grenuille FROG from Swamp Optics). However, compression of the pulse to the transform limit is not necessary at this point in the system.

The oscillator is phase locked to a sub-harmonic of the NIF master clock. To achieve this, 1% of the output signal from the oscillator is tapped off from the main output beam and sent to a photodiode. This signal is then RF filtered to pass only the fundamental harmonic at 38.88MHz. The filtered signal is compared to an electronically phase shifted signal from the master clock via a phase comparator. (The electronic phase shifter allows the pulse timing to be adjusted by up to 1 cavity round trip: beyond that a different pulse can be selected for timing.) This generates an error signal proportional to the phase error. A phase locked loop control circuit then feeds a fast and slow correction signal back to the two actuators on the linear stages inside the cavity.

A second photo-diode, RF bandpass filter and phase comparator were set up at the oscillator output. The RMS voltage at the output of the second phase comparator indicated that the phase noise was less than 8 ps RMS. This was also verified by analyzing the phase comparator output with an RF spectrum analyzer and integrating the RF output spectrum from the phase comparator (no signal was observable above the noise floor beyond 1.5kHz). The 8 ps RMS value was also consistent with the size of the error signal from the phase locking circuit. The mode-locked operation was very robust in the geometry pictured in figure 2b.

The mode-locked oscillator now runs 24 hours a day, 7 days a week for months at time with no interruption of either mode-locking or phase locking.

A fiber coupled acousto-optic modulator (AOM) at the oscillator output reduces the pulse repetition rate to 200 kHz. The AOM has a time window of 25 ns, which is sufficient to select a single pulse from the oscillator pulse train. The pulse train at the AOM output has an average power of 28 μW, which includes some leakage from the AOM and thus is not an accurate reflection of the pulse energy at this point in the system.

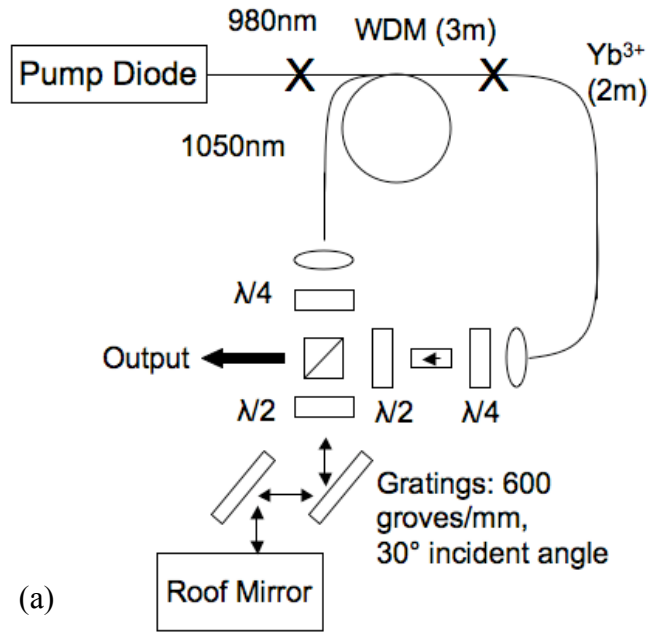

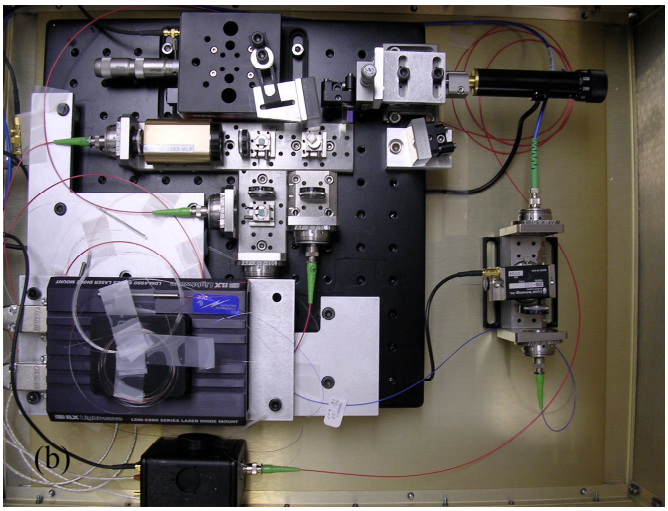

Fig. 2. (a) Schematic of the fiber mode locked oscillator (b) picture of the assembled oscillator viewed from the top

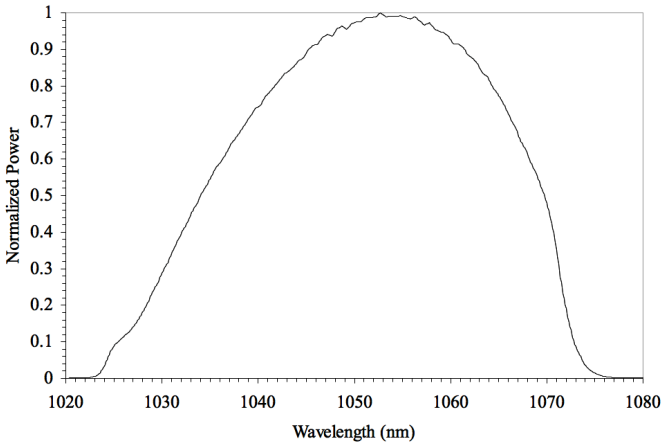

Fig. 3. Spectrum from mode locked oscillator taken with an ANDO Optical Spectrum Analyzer with a resolution bandwidth of 0.1 nm.

B. *Compressed Pulse Amplifier*

The pulses from the output of the oscillator AOM propagate through 40 m of polarization maintaining (PM) fiber having a mode field diameter of 6.6 µm. This intentionally stretches the pulses to about 40 ps so they can be amplified without distortion to 205 nJ in the compressed pulse amplifier that follows.

The compressed pulse amplifier consists of two-stages. The first stage is assembled (fusion spliced) from a PM SIFAM 976/1053nm WDM (part number FPW-98005310), a 500mW JDS Uniphase 976nm grating stabilized pump diode laser and 4-5m of Nufern PM Yb^{3+} doped fiber (part number PM-YSF-HI-V2) with a mode field diameter of 7.5µm and a pair of FC/APC PM fiber connectors. An AOM following the first stage maintains the 200kHz pulse train and removes residual noise left by the first AOM. The power at this point is 1.08mW, implying 5.4 nJ pulses. A fiber-coupled isolator with an integrated 15nm band pass filter follows the AOM. The second stage PM amplifier was purchased from Nufern (part number PASA-25-250-976-SC200-1P). This was custom built to LLNL specifications. The compressed pulse amplifier's second stage amplifier is identical to fiber amplifiers 3a and 3b and contains the fiber described at the end of the self phase modulation section III-C. The output of the second stage exits the amplifier via a 0.5m armored cable terminated with an SMA connector.

C. *Pulse Compressor and ASE Pulse Cleaner*

The beam from the output of the compressed pulse amplifier is collimated to 1mm diameter and passed through a first pulse compressor, which is constructed from two 1200g/mm gratings from Newport Corporation with an angle of incidence of 45 degrees and a slant distance between the gratings of 16 cm. The compressor's GDD is -1.37 ps^2/rad and the TOD is 0.0046 ps^3/rad^2. The spectrum at this point is approximately 12nm FWHM centered at 1053nm, with a slight bias to the blue side due to the shorter fiber length in second stage of the compressed pulse amplifier. A FROG measurement confirmed compression to 268 fs.

The output beam from the pulse compressor was temporally-cleaned by focusing it through a resonant saturable absorber module made by BATOP (part number FS-SANOS-1064-2). The angle of incidence was adjusted to optimize the operation at 1053nm. The pulse cleaner had a nominal FWHM bandwidth of 17nm and a 20dB bandwidth of 5nm. It was specified to provide a 20dB pulse contrast enhancement with a 75% insertion loss and a saturation fluence of 8µJ/cm^2. A FROG measurement confirmed the pulse width was unchanged at 268 fs.

The ASE pre-pulse contrast ratio was measured before and after the pulse cleaner using a photo-diode and a set of calibrated neutral density filters. First the beam was focused onto the photo-diode such that the ASE pedestal within the AOM window, but preceding the pulse could be clearly seen on an oscilloscope. This permitted a measurement of the photodiode voltage corresponding to the ASE power, though the signal corresponding to the pulse peak was saturated. Neutral density filters were then added prior to the photo-diode until the impulse response of the photo-diode/oscilloscope combination was observed (400 ps); at this point the peak power of the pulse could be determined. The ratio of this voltage and the ASE voltage was calculated and multiplied by the optical density of the neutral density filters employed as well as by the ratio of the photodiode/oscilloscope impulse response to the desired pulse width (1 ps not the measured 268fs as the pulse still has too much bandwidth). An example set of data is shown in Fig. 4.

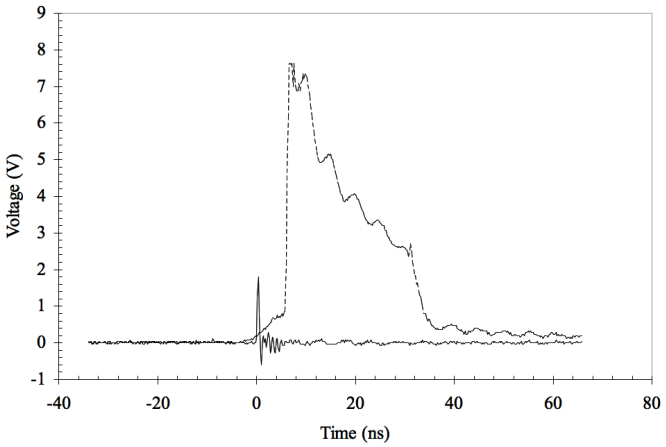

Fig. 4. Data from pre-pulse contrast measurement at input to the ASE pulse cleaner. The solid line is the attenuated pulse and the dashed line is the unattenuated pulse. The ASE pedestal is clearly visible in the unattenuated pulse as a foot prior to the rapidly rising main edge of the unattenuated pulse.

Following the procedure outlined above, the pre-pulse contrast prior to the pulse cleaner was measured to be 64dB. Following the pulse cleaner the contrast was measured to be 73dB. However, the pulse still contains both signal and ASE outside of the target 5nm bandwidth at this point in the system. This out-of-band ASE is also out of the 20dB FWHM of the SANOS pulse cleaner and will be eliminated by the CFBG. This measurement will be done again after recompression of the fully amplified pulses and shown to have 78dB of final pre-pulse contrast.

The average power at the output of the pulse cleaner was measured to be 9.8mW with a pulse repetition rate of 200kHz. Given the high measured signal to noise ratio at this point, it can be concluded with high confidence that the energy per pulse is 49nJ. The pulse spectrum at the output of the pulse cleaner is shown in figure 5. The spectrum has a flat region in relatively flat region in the center corresponding to the maximum loss in the resonant saturable absorber. The peaks to either side are predominantly due to the pulse, but likely contain some ASE that was not removed by the cleaner. The peaks will be removed by the CFBG.

After the pulse cleaner, the pulse traverses the pre-stretcher (see section III-A). The pulse energy after the pre-stretcher is 35 nJ and the spectra is unchanged.

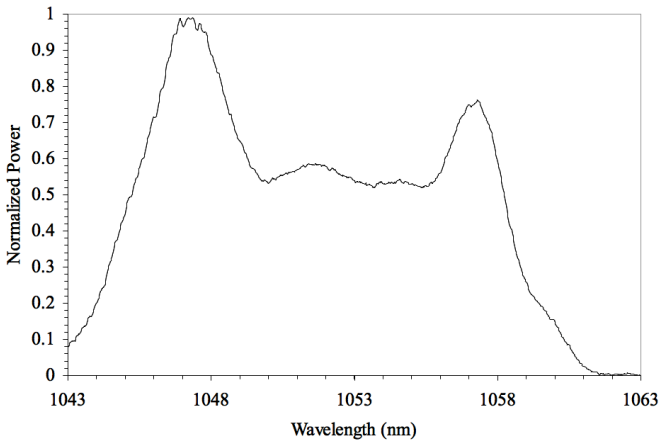

Fig. 5. Spectra from the pulse cleaner output at 49 nJ per pulse.

D. Chirped Fiber Bragg Grating

The CFBG was custom made by the University of Southampton to an LLNL specification based upon the dispersion estimate discussed in section III-A. The nominal length is 30cm, and the grating reflectance is 50%. An earlier investigation found that higher reflectivity created strong wavelength dependent losses. 50% reflectivity was determined to be a good compromise between the wavelength dependent loss and the overall component loss.

The CFBG dispersion was validated by the RF phase shift method [22]. The GDD was measured to be 310.5 ps^2/rad and the TOD to be -3.912 ps^3/rad^2. Recall that the CFBG was specified to have a GDD of 313.0 ps^2/rad and a TOD of -4.849 ps^3/rad^2, implying that the CFBG met its targets.

The CFBG was not recoated after it was manufactured, so it is very sensitive to mechanical perturbations. To help protect the fiber a single mode pigtail 0.5m long with an FC/APC connector on one end was fusion spliced onto its lead end. The CFBG was then carefully laid out straight in mechanical housing and strain relieved at the input end.

The CFBG is the only component in the system not made from PM fiber. The fiber has a mode field diameter of 4.7 µm and exhibits significant birefringence. The pulses are coupled to the CFBG using a circulator configuration consisting of a polarizing beam splitter (OFR part number PSCL-B-VR-1053), a Faraday rotator (OFR part number IOB-3D-1053-I) and two fiber ports (OFR part numbers PAF-X-5-1053, PAF-X-7-1053). A quarter and half waveplate prior to the launch into the CFBG permit the compensation of the birefringence such that the pulse illuminates only one polarization eigenaxis of the CFBG. 35nJ pulses are incident on the CFBG circulator configuration with coupling losses, CFBG losses and spectral clipping 1nJ stretched pulses are coupled into the PM fiber patch cord at the output of the CFBG-circulator. Figure 6a shows the spectra at the output of the CFBG measured with an ANDO optical spectrum analyzer with 0.1nm resolution bandwidth. Figure 6b shows the temporal profile of the pulse at the output of the CFBG measured with a 10GHz photo-diode and oscilloscope.

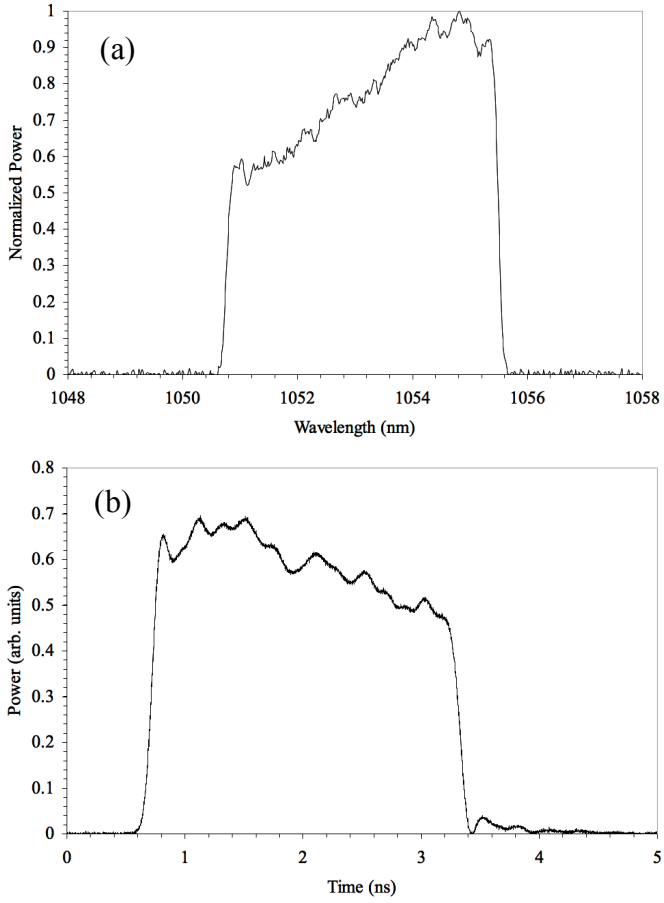

Fig. 6. Output of CFBG (a) spectral output measured with ANDO optical spectrum analyzer with 0.1nm resolution bandwidth (b) temporal output measured with 10GHz photo-diode and oscilloscope.

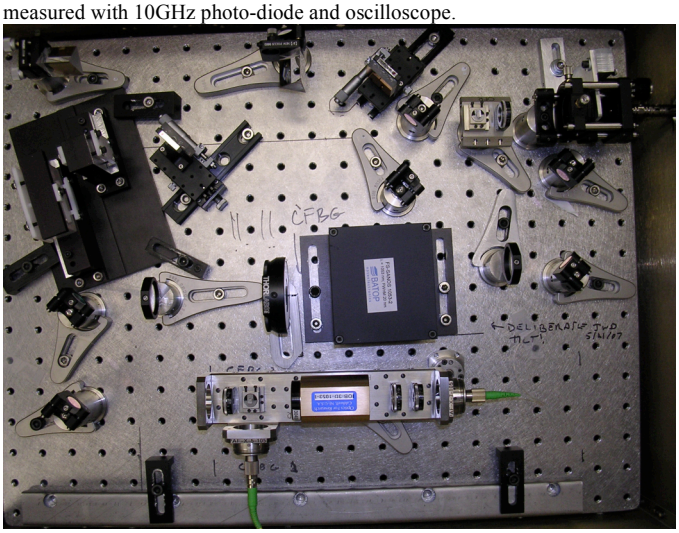

Fig. 7. Top view of the compressor, pulse cleaner, pre-stretcher and CFBG.

The pulse compressor, pulse cleaner, pre-stretcher and CFBG/circulator were mounted on a 2" thick optical breadboard that could be rack mounted in a standard 19" rack. A top view picture of the assembly is shown in figure 7. The fiber launch is the black assembly in the upper right hand corner of the picture. The collimated beam propagated through a waveplate and 15nm bandpass filter prior to entering the pulse compressor. The pulse compressor consists of the two gratings and roof mirror in the upper middle portion of the picture. The pulse compressor roof mirror lowers the beam

height and flat 0.5" mirror turns the lowered return beam 90 degrees prior to the bandpass filter. A set of three similar mirrors bring the beam back to the center right of the picture and send it propagating to the left. At this point it is focused by the far left lens through the BATOP pulse cleaner (the black box in the center of the picture). The pulse then propagates through a ½ waveplate and is recollimated by a second lens. It is then turned upwards by another 0.5" mirror and propagates through the pre-stretcher; two gratings mounted on the black rectangle in the upper left hand corner of the picture and the roof mirror in the very top left hand corner of the picture. The pre-stretcher roof mirror raises the beam height back up so that it passes over the 0.5" injection mirror and is redirected by a final 0.5" turning mirror into the circulator configuration seen in the bottom of the picture. The Faraday rotator is the gold box. The CFBG is contained in the rectangular metal housing at the very bottom of the picture. Photo-diodes were embedded after this picture was taken in order to provide an in chassis diagnostic of the operating system. The photo-diodes are positioned to collect the zero order light from the first pulse compressor grating and the second pre-stretcher grating.

E. Amplifier Chain

The 1nJ stretched pulse from the CFBG propagates through a PM patch cord to the split beam amplifier (SBA). The SBA is the same design as the first stage amplifier from the CPA. The split beam amplifier is followed by a OFR isolator containing a 5nm bandpass filter centered at 1053nm. This in turn is followed by an AOM that reduces the pulse repetition rate from 200kHz to 10kHz. The SBA can amplify pulses from 1nJ up to as high as 78nJ through the AOM. There is a 0.5m PM patch cord connecting the AOM to a 50% beam splitter that splits the pulses into two patch cables that will lead to the pulse tweaker.

The pulse tweaker is not yet available, since its final design requires more precise knowledge of the system's dispersion. Today then, the amplified pulses are coupled directly to the 120m long cabled transport fibers and the SBA is operated at a diode pump power consistent with 1nJ pulses in the transport fibers. When the tweakers are added to the system the loss will likely increase requiring the SBA to be operated at higher gain.

The output of the transport fibers is coupled into a 99%/1% splitter. The 1% port of this splitter is coupled to a photo-diode for use as a diagnostic. The 99% port is coupled to the input of fiber amplifier 2.

Fiber amplifier 2 is pumped with a 1.5W, 976nm laser diode coupled to a 100μm/0.22NA fiber (Axcel Photonics part number B1-975-1500-15A). This fiber is fusion spliced to the pump arm of a pump signal combiner (Nufern), which precedes the gain fiber (discussed in section III-C). The signal arm of the pump signal combiner was mode matched to the 11μm core gain fiber. Fiber amplifier 2 amplifies the pulse from 1nJ to 1μJ.

The output of the pump signal combiner is coupled to an OFR optical isolator with an integrated 15nm band pass filter. The output of this device is coupled into a PM amplifier supplied by Nufern (part number PASA-25-250-976-SC200-1P). This is a custom amplifier built to LLNL specifications and is nominally the same as the second stage amplifier of the compressed pulse amplifier. This amplifier produced 100μJ pulses at the collimated output measured after collimation with an 8mm objective, an iris (to eliminate cladding and pump light) and optical isolator. Spectra from arms A and B at 100μJ is shown in figure 8A and lower pulse energy spectra are shown in figure 8B. The pulse energies were determined by measuring the average power of the beam with a thermal power meter and then taking the spectra over a 100nm span and evaluation via integration of the spectra the fraction of the power contained in the signal band. This varied for the two amplifiers slightly as can be seen in figure 8A in that one spectra is increasing more rapidly at 1048nm than the other spectra.

The most obvious and surprising feature in figure 8A is the strong spectral ripple. Since it is the same for both amplifiers, it seems its source is common to both arms of the system and thus arose prior to the splitter. Further, note that the low energy plot, shows significantly less spectral ripple. This phenomena was investigated extensively. Attempts to correlate it to polarization holding or etalon effects failed. Polarization holding was generally in the range of 25-30dB as care was taken to exclusively use fusion splicing or micro-optic connections between fibers. The micro-optic connections included ½ waveplates to optimize the polarization holding. So far as could be determined the spectral ripple was exclusively a function of accumulated B-integral and could be observed in any of the components providing sufficient SPM could be generated. For example, increasing the SBA output to higher powers such that 25-40nJ was propagated through the transport fiber or driving fiber amplifier 2 to higher than 1μJ pulse energies generated spectra similar to that of figure 8A even before the pulses passed through final amplifier 3.

F. Fail-Safe Circuit

In any high gain fiber amplifier chain there is a possibility that one or more amplifiers may self Q-switch if their seed is lost leading to extensive damage. To prevent this the overall system includes a fail-safe circuit that monitors photodiodes at various points in the system as well as from the phase locking circuit. If phase locking or the pulse train is lost for any reason the amplifier chain is quickly shut down.

V. System Level Recompression Data

As discussed above, the tweaker design requires precise knowledge of the completed system dispersion. Towards this end, pulses from one arm of the system were recompressed with a double-passed Treacy compressor. The output of fiber amplifier 3 was collimated with a 8mm, 0.5NA asphere that permitted collection of residual pump light from the amplifier output. This beam passed through an iris to remove pump light, a half waveplate, an optical isolator and a 15nm band pass filter. These components ensured only signal light was launched into the compressor and protected the amplifier

chain from optical feedback. A telescope with a -100mm and +150mm focal length lens resized the beam to 6mm diameter in order to ensure it had the required 12m Rayleigh range needed to pass through the compressor essentially unchanged. The telescope also put the collimated beam waist approximately in the center of the compressor path.

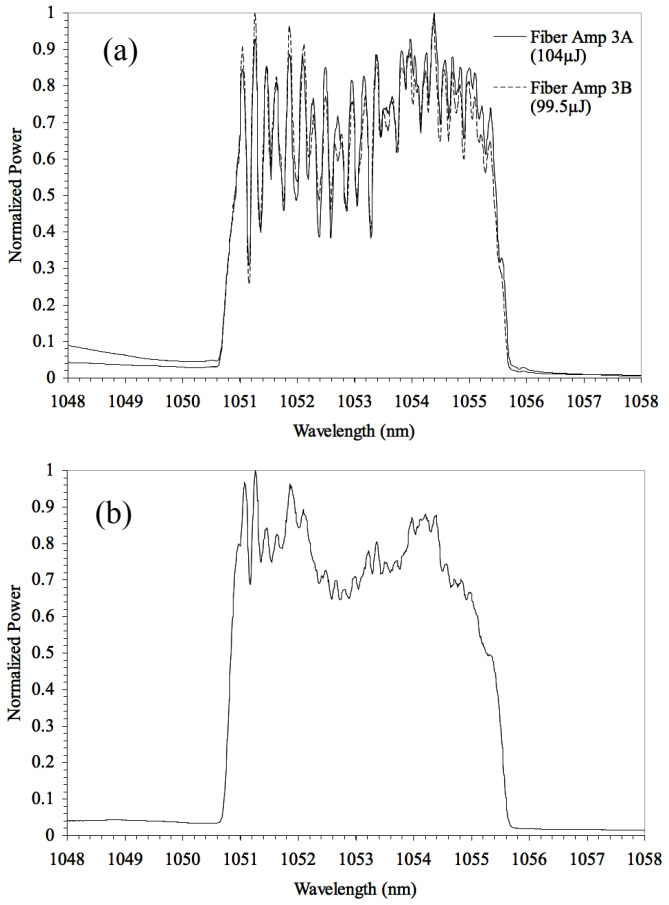

Fig. 8. Output of fiber amplifiers 3A and 3B (a) spectral output measured with ANDO optical spectrum analyzer with 0.1nm resolution bandwidth at approximately 100μJ (b) spectral output of fiber amplifier 3B at 2.3μJ corresponding to B=1.5.

The compressor was constructed from of an LLNL multilayer dielectric grating with a groove density of 1784g/mm and an angle of incidence of 74.2 degrees resulting in a GDD of -319.26 ps^2/rad and TOD of 5.84 ps^3/rad^2. The GDD and TOD were determined both from knowledge of the compressor geometry and an independent measurement of the compressor dispersion made using tunable laser/RF phase measurement technique [22].

The angle of incidence and grating spacing were optimized using the following procedure. First the compressor was set at an angle of incidence and grating spacing expected to correctly compress the pulse. Second, the compressed output pulse characteristics were measured using a high-resolution frequency resolved optical gating technique (FROG), described below. Then using knowledge of the pulse residual group delay obtained from the FROG, it was possible to calculate the optimum grating angle of incidence and spacing needed to completely eliminate the lower order terms in the group delay. This procedure led the compressor result detailed above.

The output pulses were measured using a background free auto-correlator that included a delay mirror on a long travel translation stage. The second harmonic output of the auto-correlator was coupled to a single mode optical fiber and the spectrum was recorded at each delay setting over the range in which there was detectable signal light using an ANDO optical spectrum analyzer. To ensure accuracy, the measured spectrum at each point was integrated to determine a total power at each delay point. This integrated power vs. delay could be compared to the background free auto-correlation taken by placing a large area power meter in place of the fiber coupling stage. This ensured light was not being lost in the fiber coupling set-up as the stage was moved across a long range. It was important to keep the peak pulse energy in the optical fiber low enough to avoid SPM effects distorting the measured spectrum; for 1ps pulses the energies needed to be less than 20 pJ. The spectrum resolution was 0.1nm and delay steps as small as 0.05ps could be taken if necessary.

The resulting spectrum vs. delay formed a FROG trace. This trace was converted to a 512 X 512 matrix via interpolation that could be analyzed using the principal components method [23]. An example experimental FROG trace is shown in Fig. 9 below for the case of low B-integral (B = 1.4, pulse energy = 800 nJ).

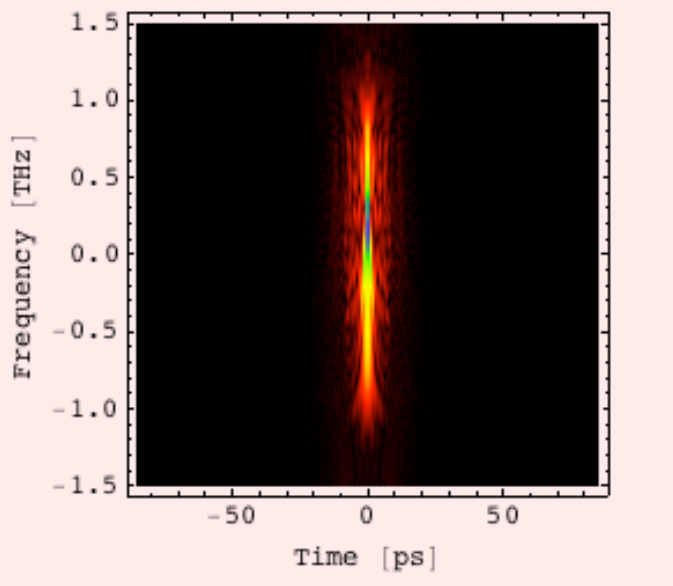

Fig. 9. High resolution experimental FROG trace of compressed 800nJ pulses with B=1.4

Pulses were characterized at 3 different output energies corresponding to a range of B-integral values. The compressor setting in terms of incident angle and grating separation were not adjusted as the energy changed. The optimal compression appears to have optimized at the same point independent of pulse energy. The pulse energy was adjusted by changing the pump power to fiber amplifier 3. The remainder of the amplifier chain was held constant. Thus even at low energy, the accumulated B-integral was 1.4. The pulses measured via the high resolution FROG are shown in Fig. 10 below. Since this FROG relies on second harmonic generation

the direction of time is unknown. Thus no weight should be put on which side of the pulses various features fall.

All of the pulses in Fig. 10 have been normalized to contain the intensity on a scale from 0 to 1. The baseline of the pulses has been shifted by 0.25 for each pulse in order to separate the baselines and make the small features around each pulse clearly visible. If the pulses were plotted on a log scale, significant (>10^{-8}) features would be visible out to +/-75 ps. Nevertheless, an integration of the pulses vs. time shows that in the 800nJ case, 80% of the energy is in the main pulse. This drops to 75% for the 58 µJ case and 65% for the 97 µJ case. On a linear scale no features are observable outside of the plotted range.

The residual group delay from the same three pulses is shown in Fig. 11 below. The 5nm wide spectrum comprises 1.3THz in frequency. The FROG measurement spanned 3THz. However, information outside the 1.3THz frequency window in which actual power is contained is not meaningful. Thus Fig. 11 plots only the frequency span from +/-0.7THz. Again the data from the three pulses has been shifted for clarity.

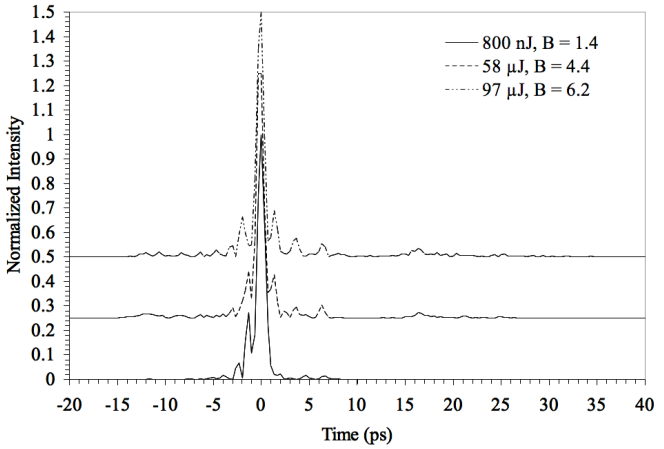

Fig. 10. Output pulses from the fiber injection laser system measured using a high resolution FROG.

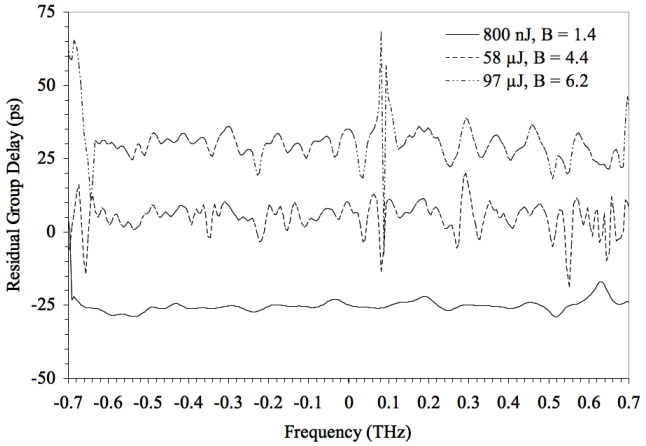

Fig. 11. Residual group delay from the output pulses of the fiber injection laser system measured using a high resolution FROG. Only data where the spectral intensity was significantly above background (>5%) has been plotted.

The first thing to note regarding the three residual delay curves in Fig. 11 is that there does not appear to be any significant low order terms. This strongly suggests that the compressor settings in terms of GDD and TOD were indeed optimized. The second thing to note is large rapid variation of the group delay ripple with frequency. This ripple grows with increasing B-integral. The 800 nJ data has a peak to peak variation of around +/- 4ps that can be attributed to group delay ripple in the CFBG. As the pulse is amplified and undergoes increasing B-integral, this ripple amplitude grows and appears to increase in frequency. In the 58 µJ case, the group delay ripple has a peak to peak variation of +/- 15ps. The 97 µJ data is not too much worse with the exception of the strong spike at around 0.08 THz.

The FROG measurement also recovered the pulse spectrum and this spectrum agreed reasonable well with the directly measured pulse spectrum. As an example Fig. 12 shows the 58µJ pulse spectrum at the input of the compressor as well as the retrieved spectrum from the FROG measurement.

One additional test was performed on the output pulses. The pre-pulse ASE contrast ratio of the output pulses was measured using the technique detailed in section IV-C above. At 97 µJ output pulse energy the ASE pre-pulse power contrast ratio for 1 ps pulses was measured to be 78 dB. This is slightly higher than the pre-pulse contrast ration measured at the output of the ASE pulse cleaner. The increase is attributed to the elimination of spectral components outside of the 20 dB bandwidth of the pulse cleaner.

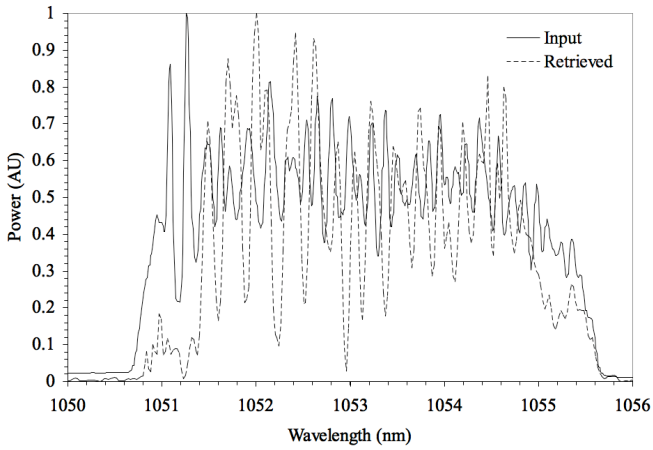

Fig. 12. Comparison of the measured and retrieved pulse spectrum for the 58 µJ pulses.

The final observation is that the pulses measured here equally weight all spectral components at the output of the injection laser system. The NIF amplifier chain will gain narrow the pulse spectra to 2.2 nm FWHM and should reduce the pedestal, improving the pulse quality and increasing the pulse contrast ratio further.

VI. Tweaker Design

At this point in time, the dispersion of the pulse exiting the injection laser system is known to have a dispersion a GDD = +319.26 ps^2/rad and a TOD = -5.84 ps^3/rad^2 (see section V). The ARC compressor dispersions were altered from the original design point in order to better fill the NIF aperture with the split beams after the initial dispersion estimate was made. This resulted in an A compressor and a B compressor that will require A and B pulse tweakers with different dispersions in order to achieve a net zero dispersion in the system. The A compressor has a design GDD = -290.10 ps^2/rad and TOD = 4.44 ps^3/rad^2. Pulse tweaker A thus needs

to make up the difference between the dispersion of the output pulse and compressor A. Thus the dispersion of pulse tweaker A needed to make the shortest possible pulse is GDD = -29.16 ps^2/rad and TOD = 1.4 ps^3/rad^2. Similarly ARC compressor B has a design dispersion of GDD = -273.71ps^2/rad and TOD = 4.03 ps^3/rad^2. Pulse tweaker B then needs a dispersion of GDD = -45.56 ps^2/rad and TOD = 1.81 ps^3/rad^2 to make the shortest pulse. In order to achieve a positively chirped pulse of 60 ps, the GDD of tweaker A must be reduced to -13.86 ps^2/rad and the GDD of tweaker B must be reduced to -30.26 ps^2/rad. Once the pulse is stretched that far in time, the TOD becomes effectively irrelevant.

The pulse tweakers will have two long travel stages. One stage will simply be a delay arm capable of providing up to 3ns of delay with ps resolution and compensating for movement of the second arm that will vary the dispersion of the system. The second arm will be a small Traecy compressor constructed from two multilayer dielectric gratings constructed at LLNL. The Traecy compressor equations for GDD and TOD as a function of grating groove density, angle of incidence and laser wavelength are well known [24]. For reference the angle of incidence (θ_{in}) and output angle (θ_{out}) for a single frequency light beam of wavelength λ, striking a grating with groove density G are related by the equation

$$\sin(\theta_{in}) + \sin(\theta_{out}) = \lambda \cdot G \tag{5}$$

The most striking attribute of the pulse tweaker dispersion requirements is the relatively large value of the TOD compared to the GDD required to compress the pulse to its minimum pulse width. That is the TOD to GDD ratio is relatively large in value. The groove density of the gratings used and the angle of incidence of the input beam determine the ratio of the TOD to the GDD in a Traecy compressor design. The TOD/GDD ratio for pulse tweaker A is -0.048 ps and for pulse tweaker B is -0.040 ps. Equation 6 below is an analytical formula for the TOD/GDD ratio of the Traecy compressor

$$\frac{TOD}{GDD} = \frac{-3\lambda}{2\pi c}\left(1 + \lambda \cdot G \frac{\sin(\theta_{out})}{\cos^2(\theta_{out})}\right) \tag{6}$$

where c is the speed of light. This can be reformatted as

$$\frac{\sin(\theta_{out})}{1 - \sin^2(\theta_{out})} = \frac{-1}{\lambda \cdot G}\left(1 + \frac{2\pi c}{3\lambda} \cdot \frac{TOD}{GDD}\right) \tag{7}$$

which is quadratic in terms of $\sin(\theta_{out})$ and thus can be solved in terms of λ, G and TOD/GDD. For the case of pulse tweaker A the angle of incidence (AOI), output angle (AOE) and Littrow angle as a function of grating groove density are plotted in Fig. 13. An interesting feature observable in figure 13 is that the angle of exit does not vary significantly with groove density. Further, the divergence of a pulse with 5nm spectral width also does not vary significantly with grating groove density over the plotted range. As a result the grating separation required to achieve zero net dispersion also does not vary significantly with groove density over the plotted range.

At groove densities higher than 1860g/mm the AOI needed to achieve the required TOD/GDD ratio is greater than 90 degrees. The multilayer dielectric gratings that will be used are most efficient (nearly 95% diffraction efficiency) at Littrow and efficiency is an important requirement for the system. Further LLNL is not set up to quickly and cheaply produce gratings with groove densities less than 1740g/mm and thus lower groove densities are not considered in the plot. Clearly the compressor cannot be physically constructed with reflection gratings with the AOI equal to the Littrow angle. To this end 1780g/mm was choosen as the grating groove density for use in the pulse tweaker. This groove density is made regularly at LLNL and thus is readily available and is close enough to Littrow to allow high efficiency operation of the multilayer dielectric gratings while being far enough from Littrow to permit a physical design that avoids the beam being clipped by the size of the gratings required or overlapping itself. This groove density corresponds to an AOI of 65.17 degrees for tweaker A. To achieve the shortest pulse the slant distance between the gratings needs to be 14.6cm and to achieve the longest (positively chirped) pulse the distance between the gratings needs to be 6.9cm. Tweaker B will also be constructed from 1780g/mm gratings, but with an AOI of 66.17 degrees. To achieve the shortest pulse for tweaker B the slant distance between the gratings needs to be 27.6cm and to achieve the longest (positively chirped) pulse the distance between the gratings needs to be 18.3 cm.

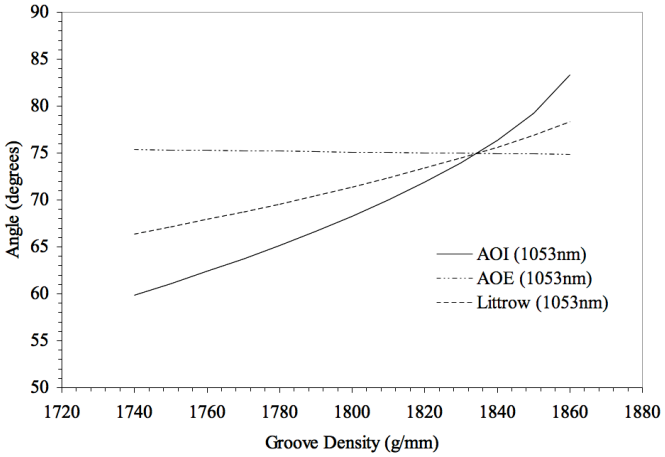

Fig. 13. Angle of incidence (AOI), output angle (AOE) and Littrow angle at 1053nm as a function of groove density for a Traecy compressor with the TOD/GDD ration needed to construct pulse tweaker A.

At the time of this writing pulse tweakers A and B have not yet been physically realized. However, an optical layout of the beam path shows that they will fit on a 2" thick optical breadboard with the same dimensions as the pulse cleaner CFBG breadboard shown in Fig. 7. This will permit them to be rack mounted in a standard 19" rack.

VII. Conclusions

A optical fiber laser system suitable for seeding a large glass laser system such as NIF has been designed and constructed. Critical issues such as dispersion, B-integral and pre-pulse contrast have been analyzed and understood. The

system has been physically realized and measured. It has been shown that critical requirements can be met. Barriers to better pulse quality are group delay ripple in the CFBG and large B-integral associated with high energy pulse amplification in optical fibers. It is noted that larger mode field diameter amplifying fibers have become available since this work was undertaken and thus the same pulse energies could be achieved with lower effective B-integral (and thus better pulse quality). Alternatively higher pulse energies could be obtained with the same B-integral. A compact pulse stretcher with low or no group delay ripple would be a desirable upgrade to the system. It is anticipated that the system will be deployed on NIF as part of the ARC system in late 2009.

ACKNOWLEDGMENT

The authors would like to thank the following people at LLNL for advice, assistance and support of Greg Tietbohl, Antonio Lucienetti, Gordon Brunton, Dave Fittinghoff, Dick Hackel, Gaylen Erbert, Don Browning and Ernesto Padilla in preparing this work. The authors would also like to thank Morten Ibsen of the University of Southampton for fabrication of the CFBGs used in this work and David Richardson and Jonathan Price also of the University of Southampton for helpful discussions. Additionally the authors would like to thank Dr. Frank Wise of Cornell for helpful discussions relating to the mode-locked fiber oscillators.

REFERENCES

[1] Y. Jeong, J. Sahu, D. Payne, J. Nilsson, "Ytterbium-doped large-core fiber laser with 1.36 kW continuous-wave output power," Opt. Express 12, 6088-6092 (2004).

[2] G. Bonati, H. Voelckel, T. Gabler, U. Krause, A. Tünnermann, J. Limpert, A. Liem, T. Schreiber, S. Nolte, and H. Zellmer, "1.53 kW from a single Yb-doped photonic crystal fiber laser," Photonics West, Late Breaking Developments, Session 5709-2a (The International Society for Optical Engineering , 2005).

[3] V. Gapontsev, D. Gapontsev, N. Platonov, O. Shkurkhin, V. Fomin, A. Mashkin, M. Abramov and S. Ferin, "2 kW CW ytterbium fiber laser with record diffraction limited brightness," in Proceedings of the Conference on Lasers and Electro-Optics Europe, (Optical Society of America, 2005)

[4] J. Dawson, M. Messerly, R. Beach, M. Shverdin, E. Stappaerts, A. Sridharan, P. Pax, J. Heebner, C. Siders and C. Barty, "Analysis of the scalability of diffraction-limited fiber lasers and amplifiers to high average power," Optics Express, vol. 16, pp. 13240-13266 (2008)

[5] C. Brooks and F. di Teodoro, "Mulitmegawatt peak-power, single-transverse-mode operation of a 100 μm core diameter, Yb-doped rodlike photonic crystal fiber amplifier," Applied Physics Letters, vol. 89, pp. 111119, (2006)

[6] C. Haynam, et al., "National Ignition Facility laser performance status," Applied Optics, vol. 46, pp. 3276-, (2007)

[7] D. Strickland and G. Mourou, "Compression of amplified chirped optical pulses," Opt. Commun. 56, 219-221 (1985)

[8] C. Barty, et al., "An overview of LLNL high-energy short-pulse technology for advanced radiography of laser fusion experiments," Nuclear Fusion, vol. 44, pp. S266-S275 (2004)

[9] M. Tabak, et al., "Ignition and high-gain with ultra-powerful lasers," Phys. Of Plasmas, vol. 1, pp. 1626-1634 (1994)

[10] L Shah, M. Fermann, J. Dawson, C. Barty, "Micromachining with a 50 W, 50 μJ subpicosecond fiber laser system," Optics Express, vol. 14, pp. 12546-12551 (2006)

[11] L. Shah, A. Arai, S. Eaton, P. Herman, "Waveguide writing in fused silica with a femtosecond fiber laser at 522nm and 1 MHz repetition rate," Optics Express, vol. 13, pp. 1999-2006 (2005)

[12] F.Ilday, J. Buckley, H. Lim, F. Wise and W. Clark, "Generation of 50-fs, 5-nJ pulses at 1.03 μm from a wave-breaking free fiber laser," Optics Letters, vol. 28, pp. 1365-1367, (2003)

[13] J. An, D. Kim, J. Dawson, M. Messerly, C. Barty, "Grating-less, fiber-based, oscillator that generates 25 nJ pulses at 80 MHz, compressible to 150 fs," Optics Letters, vol. 32, pp. 2010-2012 (2007)

[14] B. Ortac, O. Schmidt, T. Schreiber, J. Limpert, A. Tunnermann and A. Hideur, "High-energy femtosecond Yb-doped dispersion compensation free fiber laser," Optics Express, vol. 15, pp. 10725-10732 (2007)

[15] F. Roser, J. Rothhard, B. Ortac, A. Liem, O. Schmidt, T. Schreiber and J. Limpert, "131W 220fs fiber laser system," Optics Letters, vol. 30, pp. 2754-2756 (2005)

[16] F. Roser, T. Eidam, J. Rothhardt, O. Schmidt, D. Schimpf, J. Limpert and A. Tunnermann, "Millijoule pulse energy high repetition rate femtosecond fiber chirped-pulse amplification system," Optics Letters, vol. 32, pp. 3495-3497, (2007)

[17] G. Imeshev, I. Hartl, M. Fermann, "Chipred pulse amplification with a nonlinearly chirped fiber Bragg grating matched to the Treacy compressor," Optics Letters, vol. 29, pp. 679-681 (2004)

[18] E. B. Treacy, "Optical pulse compression with diffraction gratings," IEEE J. Quantum Electron. 5, 454-458 (1969)

[19] M. Perry, D. Pennington, B. Stuart, G. Tietbohl, J. Britten, C. Brown, S. Herman, B. Golick, M. Kartz, J. Miller, H. Powell, M. Vergino and V. Yanovsky, "Petawatt laser pulses," Optics Letters, vol. 24, pp. 160-162 (1999)

[20] M. Perry, T. Ditmire and B. Stuart, "Self-phase modulation in chirped pulse amplfication," Optics Letters, vol. 19, pp. 2149-2151 (1994)

[21] D. Schimpf, E. Seise, J. Limpert and A. Tunnerman, "The impact of spectral modulations on the contrast of pulses of nonlinear chirped pulse amplification systems," Optics Express, vol. 16, pp. 16664-16674 (2008)

[22] L. Cohen, "Comparison of single-mode fiber dispersion measurement techniques," Journal of Lightwave Technology, vol. 3, pp. 958-966 (1985)

[23] D. Kane, "Principal components generalized projections: a review," Journal of the Optical Society of America, vol. 25, pp. A120-A132 (2008)

[24] I. Walmsley, L. Waxer and C. Dorrer, "The role of dispersion in ultrafast optics," Review of Scientific Instruments, vol. 72, pp. 1-29 (2001)

[25] C. Giles and E. Desurvire, "Modeling Erbium-doped fiber amplifiers," IEEE Journal of Lightwave Technology, vol 9, pp. 271-283 (1991)

First A. Author (M'76–SM'81–F'87) The second paragraph uses the pronoun of the person (he or she) and not the author's

This work performed under the auspices of the U.S. Department of Energy by Lawrence Livermore National Laboratory under Contract DE-AC52-07NA27344.